Nonperturbative study of inverse symmetry breaking at high temperatures

Marcus B. Pinto*
Departamento de Física, Universidade Federal de Santa Catarina, 88040-900 Florianópolis, SC, Brazil

Rudnei O. Ramos†
Departamento de Física Teórica - Instituto de Física, Universidade do Estado do Rio de Janeiro, 20550-013 Rio de Janeiro, RJ, Brazil

(Received 8 December 1999; published 26 May 2000)

The optimized linear δ expansion is applied to multifield $O(N_1)\times O(N_2)$ scalar theories at high temperatures. Using the imaginary time formalism the thermal masses are evaluated perturbatively up to order δ^2 which considers consistently all two-loop contributions. A variational procedure associated with the method generates nonperturbative results which are used to search for parameter values for inverse symmetry breaking (or symmetry nonrestoration) at high temperatures. Our results are compared with the ones obtained by the one-loop perturbative approximation, the gap equation solutions and the renormalization group approach, showing good agreement with the latter method. Apart from strongly supporting inverse symmetry breaking (or symmetry nonrestoration), our results reveal the possibility of other high-temperature symmetry breaking patterns for which the last term in the breaking sequence is $O(N_1-1)\times O(N_2-1)$.

PACS number(s): 11.10.Wx, 11.15.Tk, 98.80.Cq

I. INTRODUCTION

The possibility that symmetries may be broken (or remain broken) at high temperatures is not new [1]. This phenomenon is usually called inverse symmetry breaking (ISB) [or symmetry nonrestoration (SNR)]. The idea of ISB (or SNR) is *per se* a very interesting one due to its possible implementation in realistic particle physics models and its consequences in the context of high-temperature phase transitions in the early Universe, with applications ranging from problems involving CP violation and baryogenesis, topological defect formation, inflation, etc. (for a short list of the different applications where SNR and ISB have been used see, e.g., Refs. [2–6]).

ISB or SNR is a direct consequence that in two or multifield theories some of the coupling constants between fields can be negative while the model is still bounded from below. This can be the case in any extension of the standard model with a large scalar sector. Under these conditions, there can be an enhanced symmetry breaking effect at high temperatures, when thermal effects are taken into account in the model. This effect is clear when one considers a one-loop analysis of the effective potential in a simple model of two interacting scalar fields or, as in Ref. [1], a $O(N)\times O(N)$ model. However, this simple analysis is too naive for two main reasons. First, at high temperatures the perturbative expansion in quantum field theory becomes, in most cases unreliable. This happens because there can be parameter regimes where powers of the coupling constants become surmounted by powers of the temperature, or due to the appearance of infrared divergences close to critical temperatures (as in field theories displaying a second order phase transition or a weakly first order transition). Second, the constrain conditions on the coupling constants, which may be important for the observation of ISB or SNR, usually requires large values for the couplings, in which case higher order loop corrections may become important as well and change appreciably the parameter space for ISB or SNR.

In order to account for the above problems of the one-loop approximation, different methods have been used to analyze the question of ISB in quantum field theory at high temperatures. The results, however, have shown to be highly controversial, either by finding no evidence for ISB or SNR or favoring the phenomenon. Examples of the former were obtained in the context of methods such as the large-N expansion [7], Gaussian effective potential [8], chiral Lagrangian technique [9], and Monte Carlo simulations on the lattice [10]. Some applications which find evidence for ISB or SNR are Refs. [11,12], whose authors worked with self-consistent gap equations; Ref. [13], also in the context of the large-N expansion, but reaching a different conclusion; Refs. [14,15] in the context of the renormalization group equations and Ref. [16], also in the context of Monte Carlo simulations but this time supporting ISB or SNR.

It is then obvious that it would be interesting to have a method to clarify this question without involving the possible difficulties related to the previous methods (such as numerical precision in the Monte Carlo simulations, self-consistency in the gap equations, or resummed perturbative methods, etc.) used to study this problem. In this paper we use a nonperturbative technique known as the linear δ expansion (also known as optimized perturbation theory) [17,18] (for earlier references see, e.g., Ref. [19]) and apply the method to the $O(N_1)\times O(N_2)$ scalar model to obtain the thermal masses to second order in the perturbative parameter δ. We then investigate their high-temperature behavior to conclude about the possibility of ISB or SNR. This model has already been considered before by Bimonte and Lozano in Ref. [11] where SNR was studied by means of the solutions of the gap equations of the model. By studying this

*Email address: fsc1mep@fsc.ufsc.br
†Email address: rudnei@dft.if.uerj.br

theory we can also extend our results to the simple model consisting of two-interacting scalar fields, which has been extensively studied before. In this case the symmetry group corresponds to $Z_2\times Z_2$. This step will allow us to compare our results with the ones furnished by alternative methods. In a previous paper [20], we have employed the optimized linear δ expansion to study the resummation of higher and leading order thermal corrections showing that the use of a proper optimization scheme is equivalent to self-consistently solving the gap equation for the thermal mass, where leading and higher order infrared regularizing contributions are nonperturbatively taken into account. An advantage of the linear δ expansion is that the same simple propagator is used in the evaluation of any diagram, avoiding the potential bookkeeping problems associated to other resummation methods. Apart from being a powerful nonperturbative method, the optimized perturbation theory was originally formulated as a general theory applicable to arbitrary systems including strong interacting models, which makes it particularly interesting to use in connection with ISB or SNR where the issue of large coupling constants is an important one.

This work is organized as follows. In Sec. II we introduce the model and the lowest order one-loop result. In the same section, the linear δ-expansion technique is briefly described. It is then used, in Sec. III, to evaluate the thermal masses up to order-δ^2 in the $3+1d$ model of interacting scalar fields with global $O(N_1)\times O(N_2)$ symmetry. These calculations explicitly include two-loop momentum independent as well as momentum dependent diagrams with equal and different internal propagators. In Sec. IV we present our optimization results for the thermal masses and investigate, numerically, the possibility of ISB in the model. We specialize to the case $N_1=90$ and $N_2=24$, where the model can be thought as representing the Kibble-Higgs sector of a SU(5) grand unified theory and also to the case $N_1=N_2=1$, where it reduces to the $Z_2\times Z_2$ model, which has been the object of many studies in connection with ISB. Our predictions for the critical temperatures and size of the ISB parameter region are compared with the ones found in the literature. In Sec. V our concluding remarks are given. Two appendices are included to present some technical details and for a brief discussion of renormalization in the model.

II. THE LINEAR δ EXPANSION APPLIED TO THE EVALUATION OF THE THERMAL MASSES IN THE $O(N_1)\times O(N_2)$ MODEL

A. The model and one-loop results

In this work we consider the scalar $O(N_1)\times O(N_2)$ model described by

$$\mathcal{L}=\sum_{i=1}^{2}\left[\frac{1}{2}(\partial_\mu\phi_i)^2-\frac{1}{2}m_i^2\phi_i^2-\frac{\lambda_i}{4!}\phi_i^4\right]-\frac{\lambda}{4}\phi_1^2\phi_2^2+\mathcal{L}_{\rm ct}, \tag{2.1}$$

where

$$\mathcal{L}_{\rm ct}=\sum_{i=1}^{2}\left[A_i\frac{1}{2}(\partial_\mu\phi_i)^2-\frac{1}{2}B_i\phi_i^2-\frac{1}{4!}C_i\phi_i^4\right]-\frac{1}{4}C\phi_1^2\phi_2^2 \tag{2.2}$$

represents the counterterms needed to render the model finite. Note that $\mathcal{L}_{\rm ct}$ requires an extra piece if one attempts to evaluate the thermal effective potential [21], which is not the case here. The boundness condition for the model described by Eq. (2.1) requires that the coupling constants satisfy the inequalities

$$\lambda_1>0,\quad \lambda_2>0\quad\text{and}\quad \lambda_1\lambda_2>9\lambda^2. \tag{2.3}$$

As noticed by Weinberg [1] this boundness condition allows for negative values of the cross coupling λ which may lead to the nonrestoration of symmetries at high temperatures. Another possibility is that theories which are symmetric at $T=0$ may be broken at large T due to this negative value of λ. The thermal masses for this model have been first calculated using the one-loop approximation which, at high T, gives

$$M_1^2\simeq m_1^2+\frac{T^2}{24}\left[\lambda_1\left(\frac{N_1+2}{3}\right)+\lambda N_2\right] \tag{2.4}$$

and

$$M_2^2\simeq m_2^2+\frac{T^2}{24}\left[\lambda_2\left(\frac{N_2+2}{3}\right)+\lambda N_1\right]. \tag{2.5}$$

Let us consider the interesting case where $\lambda<0$, $m_1^2>0$ and $m_2^2>0$ so that the theory is symmetric at $T=0$. Inverse symmetry breaking takes place if one chooses, for example,

$$|\lambda|>\frac{\lambda_1}{N_2}\left(\frac{N_1+2}{3}\right), \tag{2.6}$$

which makes the T^2 coefficient of M_1^2 negative while the same coefficient for M_2^2 is kept positive, due to the boundness condition. In this case, high temperatures will induce the breaking $O(N_1)\times O(N_2)\to O(N_1-1)\times O(N_2)$ at the critical temperature

$$\frac{T_c^2}{m_1^2}=24\left[|\lambda|N_2-\lambda_1\left(\frac{N_1+2}{3}\right)\right]^{-1}. \tag{2.7}$$

The one loop approximation results will be investigated numerically and compared to our results in Sec. IV.

B. The interpolated model

The optimized linear δ expansion is an alternative nonperturbative approximation which has been successfully used in a plethora of different problems in particle theory [18,20–24], quantum mechanics [25,26], statistical physics [27], nuclear matter [28], and lattice field theory [29]. One advantage of this method is that the selection and evaluation (including renormalization) of Feynman diagrams are done ex-

actly as in ordinary perturbation theory using a very simple modified propagator which depends on an arbitrary mass parameter. Nonperturbative results are then obtained by fixing this parameter. The standard application of the linear δ expansion to a theory described by a Lagrangian density $\mathcal{L}$ starts with an interpolation defined by

$$\mathcal{L}^{\delta}=(1-\delta)\mathcal{L}_0(\eta)+\delta\mathcal{L}=\mathcal{L}_0(\eta)+\delta[\mathcal{L}-\mathcal{L}_0(\eta)], \tag{2.8}$$

where $\mathcal{L}_0(\eta)$ is the Lagrangian density of a solvable theory which can contain arbitrary mass parameters (η). The Lagrangian density $\mathcal{L}^{\delta}$ interpolates between the solvable $\mathcal{L}_0(\eta)$ (when $\delta=0$) and the original $\mathcal{L}$ (when $\delta=1$). For the present model one may choose

$$\mathcal{L}_0(\eta_i)=\sum_{i=1}^{2}\left[\frac{1}{2}(\partial_\mu\phi_i)^2-\frac{1}{2}m_i^2\phi_i^2-\frac{1}{2}\eta_i^2\phi_i^2\right], \tag{2.9}$$

and following the general prescription one can write

$$\mathcal{L}^{\delta}=\sum_{i=1}^{2}\left[\frac{1}{2}(\partial_\mu\phi_i)^2-\frac{1}{2}\Omega_i^2\phi_i^2-\delta\frac{\lambda_i}{4!}\phi_i^4+\frac{\delta}{2}\eta_i^2\phi_i^2\right]-\delta\frac{\lambda}{4}\phi_1^2\phi_2^2+\mathcal{L}_{\rm ct}^{\delta}, \tag{2.10}$$

where $\Omega_i^2=m_i^2+\eta_i^2$. The term $\mathcal{L}_{\rm ct}^{\delta}$, which contains the counterterms needed to render the model finite, is given by

$$\mathcal{L}_{\rm ct}^{\delta}=\sum_{i=1}^{2}\left[A_i^{\delta}\frac{1}{2}(\partial_\mu\phi_i)^2-\frac{1}{2}B_i^{\delta}(\Omega_1,\Omega_2)\phi_i^2-\frac{1}{4!}\delta C_i^{\delta}\phi_i^4+\frac{1}{2}\delta B_i^{\delta}(\eta_1,\eta_2)\phi_i^2\right]-\frac{1}{4}\delta C^{\delta}\phi_1^2\phi_2^2, \tag{2.11}$$

where A_i^{δ}, B_i^{δ}, C_i^{δ}, and C^{δ} are the counterterms coefficients. One should note that the δ-expansion interpolation introduces only ''new'' quadratic terms not altering the renormalizability of the original theory. That is, the counterterms contained in $\mathcal{L}_{\rm ct}^{\delta}$, as well as in the original $\mathcal{L}_{\rm ct}$, have the same polynomial structure.

The general way the method works becomes clear by looking at the Feynman rules generated by $\mathcal{L}^{\delta}$. First, the original ϕ_i^4 vertex has its original Feynman rule $-i\lambda_i$ modified to $-i\delta\lambda_i$ (the same applies to the mixed vertex $\phi_1^2\phi_2^2$). This minor modification is just a reminder that one is really expanding in orders of the artificial parameter δ. Most importantly, let us look at the modifications implied by the addition of the arbitrary quadratic part. The original bare propagator

$$S(k)=i(k^2-m_i^2+i\epsilon)^{-1}, \tag{2.12}$$

becomes

$$S(k)=i(k^2-\Omega_i^2+i\epsilon)^{-1}=\frac{i}{k^2-m_i^2+i\epsilon}\left[1-\frac{i}{k^2-m_i^2+i\epsilon}(-i\eta_i^2)\right]^{-1}, \tag{2.13}$$

indicating that the term proportional to $\eta_i^2\phi_i^2$ contained in $\mathcal{L}_0$ is entering the theory in a nonperturbative way. On the other hand, the piece proportional to $\delta\eta_i^2\phi_i^2$ is only being treated perturbatively as a quadratic vertex (of weight $i\delta\eta_i^2$). Since only an infinite order calculation would be able to compensate for the infinite number of $(-i\eta_i^2)$ insertions contained in Eq. (2.13), one always ends up with a η_i dependence in any quantity calculated to finite order in δ. Then, at the end of the calculation one sets $\delta=1$ (the value at which the original theory is retrieved) and fixes η_i with the variational procedure known as the principle of minimal sensitivity (PMS) [30]

$$\left.\frac{\partial P(\eta_i)}{\partial\{\eta_i\}}\right|_{\{\bar{\eta}_i\}}=0, \tag{2.14}$$

where P represents a physical quantity calculated *perturbatively* in powers of δ.[1] This optimization procedure applied to the thermal masses will be discussed in Sec. IV.

III. THE THERMAL MASSES UP TO ORDER δ^2

We can now start our evaluation of the thermal masses, defined by

$$M_i^2=\Omega_i^2+\Sigma_i^{\delta}(p), \tag{3.1}$$

where $\Sigma_i^{\delta}(p)$ is the thermal self-energy. At lowest order (first order in δ) the relevant contributions, which are momentum independent, are given by ($i,j=1,2$ and $i\neq j$)

$$\Sigma_{i,1}^{\delta^1}(p)=-\delta\eta_i^2+\delta\frac{\lambda_i}{2}\left(\frac{N_i+2}{3}\right)\int_T\frac{d^dk}{(2\pi)^d}\frac{i}{k^2-\Omega_i^2+i\epsilon}+\delta\frac{\lambda}{2}N_j\int_T\frac{d^dk}{(2\pi)^d}\frac{i}{k^2-\Omega_j^2+i\epsilon}. \tag{3.2}$$

The temperature dependence can be readily obtained by using the standard imaginary time formalism prescription

$$p_0\to i\omega_n,\quad \int_T\frac{d^dk}{(2\pi)^d}\to iT\sum_n\int\frac{d^{d-1}\mathbf{k}}{(2\pi)^{d-1}}. \tag{3.3}$$

Then, the self-energy becomes

[1]For a discussion of convergence as well as renormalization in the method, see Ref. [20], and references therein.

$$\Sigma_i^{\delta^1}(p) = -\delta\eta_i^2 + \delta T\frac{\lambda_i}{2}\left(\frac{N_i+2}{3}\right)\sum_n \int \frac{d^{d-1}\mathbf{k}}{(2\pi)^{d-1}}\frac{1}{\omega_n^2+E_i^2} + \delta T\frac{\lambda}{2}N_j\sum_n \int \frac{d^{d-1}\mathbf{k}}{(2\pi)^{d-1}}\frac{1}{\omega_n^2+E_j^2}, \tag{3.4}$$

where $E^2=\mathbf{k}^2+\Omega^2$. Summing over Matsubara's frequencies one gets

$$\Sigma_i^{\delta^1}(p) = -\delta\eta_i^2 + \delta\frac{\lambda_i}{2}\left(\frac{N_i+2}{3}\right) \times \int \frac{d^{d-1}\mathbf{k}}{(2\pi)^{d-1}}\left\{\frac{1}{2E_i} - \frac{1}{E_i[1-\exp(E_i/T)]}\right\} + \delta\frac{\lambda}{2}N_j\int \frac{d^{d-1}\mathbf{k}}{(2\pi)^{d-1}}\left\{\frac{1}{2E_j} - \frac{1}{E_j[1-\exp(E_j/T)]}\right\}. \tag{3.5}$$

Then, using dimensional regularization [31] ($d=4-2\epsilon$) one obtains the thermal mass

$$M_i^2 = \Omega_i^2 - \delta\eta_i^2 + \delta\frac{\lambda_i}{32\pi^2}\left(\frac{N_i+2}{3}\right) \times\left\{\Omega_i^2\left[-\frac{1}{\epsilon}+\ln\left(\frac{\Omega_i^2}{4\pi\mu^2}\right)+\gamma_E-1\right] + 32\pi^2T^2h\left(\frac{\Omega_i}{T}\right)\right\} + \delta\frac{\lambda}{32\pi^2}N_j \times\left\{\Omega_j^2\left[-\frac{1}{\epsilon}+\ln\left(\frac{\Omega_j^2}{4\pi\mu^2}\right)+\gamma_E-1\right] + 32\pi^2T^2h\left(\frac{\Omega_j}{T}\right)\right\}, \tag{3.6}$$

where μ is a mass scale introduced by dimensional regularization and

$$h(y_i) = \frac{1}{4\pi^2}\int_0^\infty dx\,\frac{x^2}{[x^2+y_i^2]^{1/2}[\exp(x^2+y_i^2)^{1/2}-1]}. \tag{3.7}$$

Note that the temperature independent term diverges and must be renormalized. In this paper we chose the minimal subtraction (MS) scheme where the counterterms eliminate the poles only. At this order the only divergence in Eq. (3.6) is

$$\Sigma_{\mathrm{div,i}}^{\delta^1} = -\frac{\delta}{32\pi^2\epsilon}\left(\lambda_i\frac{N_i+2}{3}\Omega_i^2+\lambda N_j\Omega_j^2\right), \tag{3.8}$$

which is easily eliminated by the O(δ) mass counterterm

$$\Sigma_{\mathrm{ct,i}}^{\delta^1} = B_i^{\delta^1}(\Omega_1,\Omega_2) = \frac{\delta}{32\pi^2\epsilon}\left(\lambda_i\frac{N_i+2}{3}\Omega_i^2+\lambda N_j\Omega_j^2\right). \tag{3.9}$$

By looking at Eq. (3.6) one can see that the terms proportional to $\delta\lambda_i$ and $\delta\lambda$ represent exactly those that appear at first order in the coupling constants in ordinary perturbation theory except that we now have Ω_i^2 instead of m_i^2, $\delta\lambda_i$ instead of λ_i and $\delta\lambda$ instead of λ. Therefore, it is not surprising that to this order the renormalization procedure implied by the interpolated theory is identical to the procedure implied by the original theory at first order in the coupling constants.

Let us now analyze the temperature-dependent integral which is expressed, in the high-temperature limit ($y_i=\Omega_i/T\ll 1$), as [32]

$$h(y_i) = \frac{1}{24}-\frac{1}{8\pi}y_i-\frac{1}{16\pi^2}y_i^2\left[\ln\left(\frac{y_i}{4\pi}\right)+\gamma_E-\frac{1}{2}\right]+\mathcal{O}(y_i^3). \tag{3.10}$$

In principle, since η_i is arbitrary, one could be reluctant in taking the limit $\Omega_i/T\ll 1$. However, as discussed in our previous work [20], the use of both forms for the integral $h(y_i)$ does not lead to any significant numerical changes in the optimization procedure. This is also true in the present work. Then, by taking $h(y_i)$ in the high-temperature limit, one obtains the $\mathcal{O}(\delta)$ thermal mass

$$M_i^2 = \Omega_i^2 - \delta\eta_i^2 + \delta\lambda_i\left(\frac{N_i+2}{3}\right)X_i(T) + \delta\lambda N_jX_j(T) + \mathcal{O}(\delta^2), \tag{3.11}$$

where we have defined the quantity $X_i(T)$

$$X_i(T) = \frac{T^2}{24}-\frac{T\Omega_i}{8\pi}+\frac{\Omega_i^2}{32\pi^2}L(T), \tag{3.12}$$

with $L(T)$ given by

$$L(T) = \ln\left(\frac{4\pi T^2}{\mu^2}\right)-\gamma_E. \tag{3.13}$$

For notational convenience when expressing the remaining contributions to the self-energies, we also define the additional quantities $Y_i(T)$, $Z_i(0)$, $W_i(0)$,and $R_i(T)$ given by

$$Y_i(T) = -\frac{T\Omega_i}{16\pi}+\frac{\Omega_i^2}{32\pi^2}L(T), \tag{3.14}$$

$$Z_i(0) = \frac{1}{2}\left[\ln\left(\frac{\Omega_i^2}{4\pi\mu^2}\right)+\gamma_E\right]^2+\frac{\pi^2}{12}, \tag{3.15}$$

$$W_i(0) = \frac{1}{2}\left[\ln\left(\frac{\Omega_i^2}{4\pi\mu^2}\right)+\gamma_E-1\right]^2+\frac{1}{2}+\frac{\pi^2}{12}, \tag{3.16}$$

and

$$R_i(T) = -\frac{T\Omega_i^2}{16\pi\Omega_j} + \frac{\Omega_i^2}{32\pi^2}L(T). \tag{3.17}$$

At $\mathcal{O}(\delta^2)$ the self-energy receives contributions from momentum independent as well as momentum-dependent diagrams. Let us first consider the momentum-independent diagrams, which to this order have one and two loops. The order-δ^2, one loop, momentum-independent contribution is given (in the high-temperature limit) by

$$\Sigma_{i,2}^{\delta^2} = \delta^2\lambda_i\eta_i^2\left(\frac{N_i+2}{3}\right)\left[\frac{1}{32\pi^2\epsilon} - \frac{Y_i(T)}{\Omega_i^2}\right] \tag{3.18}$$

and

$$\Sigma_{i,3}^{\delta^2} = \delta^2\lambda\,\eta_j^2 N_j\left[\frac{1}{32\pi^2\epsilon} - \frac{Y_j(T)}{\Omega_j^2}\right]. \tag{3.19}$$

As discussed in Appendix B, the above contributions can be rendered finite using the mass type counterterms contained in $\mathcal{L}_{\rm ct}^{\delta}$ which are tailored to account for divergences arising from the extra quadratic vertices introduced during the interpolation process. The momentum-independent two loop contribution is given by the four ''double scoop'' diagrams

$$\begin{aligned}\Sigma_{i,4}^{\delta^2} = \delta^2\lambda_i^2\left(\frac{N_i+2}{3}\right)^2\Bigg\{&\frac{\Omega_i^2}{(32\pi^2)^2\epsilon^2} \\ &- \frac{1}{32\pi^2\epsilon}[X_i(T)+Y_i(T)] - \frac{T^3}{384\pi\Omega_i} \\ &+ \frac{T^2}{128\pi^2} + \frac{L(T)}{(16\pi)^2}\left[8X_i(T) - \frac{T\Omega_i}{2\pi}\right] \\ &+ \frac{\Omega_i^2}{(32\pi^2)^2}[Z_i(0)+W_i(0)]\Bigg\},\end{aligned} \tag{3.20}$$

$$\begin{aligned}\Sigma_{i,5}^{\delta^2} = \delta^2\lambda\lambda_i\frac{(N_i+2)}{3}N_j\Bigg\{&\frac{\Omega_j^2}{(32\pi^2)^2\epsilon^2} \\ &- \frac{1}{32\pi^2\epsilon}[X_j(T)+R_j(T)] - \frac{T^3}{384\pi\Omega_i} \\ &+ \frac{T^2}{128\pi^2}\frac{\Omega_j}{\Omega_i} + \frac{L(T)}{(16\pi)^2}\left[8X_j(T) - \frac{T\Omega_j^2}{2\pi\Omega_i}\right] \\ &+ \frac{\Omega_j^2}{(32\pi^2)^2}[Z_i(0)+W_j(0)]\Bigg\},\end{aligned} \tag{3.21}$$

$$\begin{aligned}\Sigma_{i,6}^{\delta^2} = \delta^2\lambda\lambda_j\frac{(N_j+2)}{3}N_i\Bigg\{&\frac{\Omega_j^2}{(32\pi^2)^2\epsilon^2} \\ &- \frac{1}{32\pi^2\epsilon}[X_j(T)+Y_j(T)] - \frac{T^3}{384\pi\Omega_j} \\ &+ \frac{T^2}{128\pi^2} + \frac{L(T)}{(16\pi)^2}\left[8X_j(T) - \frac{T\Omega_j}{2\pi}\right] \\ &+ \frac{\Omega_j^2}{(32\pi^2)^2}[Z_j(0)+W_j(0)]\Bigg\},\end{aligned} \tag{3.22}$$

and

$$\begin{aligned}\Sigma_{i,7}^{\delta^2} = \delta^2\lambda^2 N_i N_j\Bigg\{&\frac{\Omega_i^2}{(32\pi^2)^2\epsilon^2} - \frac{1}{32\pi^2\epsilon}[X_i(T)+R_i(T)] \\ &- \frac{T^3}{384\pi\Omega_j} + \frac{T^2}{128\pi^2}\frac{\Omega_i}{\Omega_j} + \frac{L(T)}{(16\pi)^2} \\ &\times\left[8X_i(T) - \frac{T\Omega_i^2}{2\pi\Omega_j}\right] + \frac{\Omega_i^2}{(32\pi^2)^2}[Z_j(0)+W_i(0)]\Bigg\}.\end{aligned} \tag{3.23}$$

To render these diagrams finite one needs mass and vertex counterterms [31]. Considering the $\mathcal{O}(\delta)$ mass counterterms used to eliminate the divergences in $\Sigma_{\rm div,i}^{\delta^1}$ [see Eq. (3.9)], one is able to build two one loop $\mathcal{O}(\delta^2)$ diagrams whose contributions are given by

$$\begin{aligned}\Sigma_{i,8}^{\delta^2} = &\frac{\delta^2\lambda_i(N_i+2)}{3(32\pi^2)^2}\left[\frac{\lambda_i\Omega_i^2(N_i+2)}{3} + \lambda\Omega_j^2 N_j\right] \\ &\times\left\{-\frac{1}{\epsilon^2} + \frac{32\pi^2}{\Omega_i^2}Y_i(T)\frac{1}{\epsilon} - Z_i(0)\right\}\end{aligned} \tag{3.24}$$

and

$$\begin{aligned}\Sigma_{i,9}^{\delta^2} = &\frac{\delta^2\lambda N_j}{(32\pi^2)^2}\left[\frac{\lambda_j\Omega_j^2(N_j+2)}{3} + \lambda\Omega_i^2 N_i\right] \\ &\times\left\{-\frac{1}{\epsilon^2} + \frac{32\pi^2}{\Omega_j^2}Y_j(T)\frac{1}{\epsilon} - Z_j(0)\right\}.\end{aligned} \tag{3.25}$$

Additionally, from the vertex counterterms appearing in Eq. (2.11), with C_i and C [at order $\mathcal{O}(\delta^2)$] given by

$$C_i = \frac{\delta^2}{32\pi^2\epsilon}\left[\lambda_i^2\frac{(N_i+8)}{3} + 3\lambda^2 N_j\right] \tag{3.26}$$

and

$$C=\frac{2\delta^2\lambda^2}{16\pi^2\epsilon}+\frac{\delta^2\lambda}{96\pi^2\epsilon}[\lambda_1(N_1+2)+\lambda_2(N_2+2)], \tag{3.27}$$

one can build the one-loop $\mathcal{O}(\delta^2)$ diagrams

$$\Sigma^{\delta^2}_{i,10}=-\frac{\delta^2}{16\pi^2}\frac{(N_i+2)}{3}\left[\lambda_i^2\frac{(N_i+8)}{6}+\lambda^2\frac{3N_j}{2}\right]\times\left[\frac{\Omega_i^2}{32\pi^2\epsilon^2}-\frac{1}{\epsilon}X_i(T)+\frac{\Omega_i^2}{32\pi^2}W_i(0)\right] \tag{3.28}$$

and

$$\Sigma^{\delta^2}_{i,11}=-\frac{\delta^2 N_j}{32\pi^2}\left\{4\lambda^2+\frac{\lambda}{3}[\lambda_i(N_i+2)+\lambda_j(N_j+2)]\right\}\times\left[\frac{\Omega_j^2}{32\pi^2\epsilon^2}-\frac{1}{\epsilon}X_j(T)+\frac{\Omega_j^2}{32\pi^2}W_j(0)\right]. \tag{3.29}$$

The next contribution to the self-energy at $\mathcal{O}(\delta^2)$ comes from the two-loop ''setting sun'' diagrams. These momentum-dependent contributions are given by the setting sun diagram with equal mass internal propagators

$$\Sigma^{\delta^2}_{i,12}(p)=-\delta^2\frac{\lambda_i^2(N_i+2)}{18}(G_{iii,0}+G_{iii,1}+G_{iii,2}), \tag{3.30}$$

and by the one with internal propagators with different masses

$$\Sigma^{\delta^2}_{i,13}(p)=-\delta^2\frac{\lambda^2 N_j}{2}(G_{ijj,0}+G_{ijj,1}+G_{ijj,2}). \tag{3.31}$$

In the above expressions, G_0 is the zero-temperature part of the diagrams and G_1 and G_2 are the finite-temperature ones (with one and two Bose factors, respectively). The details of the evaluation of Eqs. (3.30) and (3.31) are given in Appendix A. Their contributions are

$$\begin{aligned}\mathrm{Re}[\Sigma^{\delta^2}_{i,12}(p)]=&\,\delta^2\frac{\lambda_i^2(N_i+2)}{3(32\pi^2)^2}\left[\frac{\Omega_i^2}{\epsilon^2}+\frac{\Omega_i^2}{\epsilon}-\frac{p^2}{6\epsilon}-\frac{64\pi^2X_i(T)}{\epsilon}\right]+\delta^2\frac{\lambda_i^2(N_i+2)\Omega_i^2}{6(4\pi)^4}\left[\ln^2\left(\frac{\Omega_i^2}{4\pi\mu^2}\right)\right.\\&\left.+\left(2\gamma_E-\frac{17}{6}\right)\ln\left(\frac{\Omega_i^2}{4\pi\mu^2}\right)+1.9785\right]+\delta^2\frac{\lambda_i^2(N_i+2)}{3(4\pi)^2}\left[\ln\left(\frac{\Omega_i^2}{4\pi\mu^2}\right)-2+\gamma_E\right]\\&\times\left\{\frac{T^2}{24}-\frac{T\Omega_i}{8\pi}-\frac{\Omega_i^2}{16\pi^2}\left[\ln\left(\frac{\Omega_i}{4\pi T}\right)+\gamma_E-\frac{1}{2}\right]\right\}+\delta^2\frac{\lambda_i^2(N_i+2)T^2}{72(4\pi)^2}\left[\ln\left(\frac{\Omega_i^2}{T^2}\right)+5.0669\right],\end{aligned} \tag{3.32}$$

and

$$\begin{aligned}\mathrm{Re}[\Sigma^{\delta^2}_{i,13}(p)]=&\,\delta^2\frac{\lambda^2N_j}{2}\frac{\Omega_j^2}{(4\pi)^4}\left\{\frac{1}{\epsilon^2}\left(1+\frac{n^2}{2}\right)+\frac{1}{\epsilon}\left(1+\frac{n^2}{2}\right)\left[3-2\gamma_E-2\ln\left(\frac{\Omega_j^2}{4\pi\mu^2}\right)\right]-\frac{p^2}{4\Omega_j^2\epsilon}-\frac{n^2}{\epsilon}\ln(n^2)\right\}\\&-\delta^2N_j\frac{\lambda^2T^2}{(4\pi)^2}\frac{1}{\epsilon}\left[h\left(\frac{\Omega_i}{T}\right)+2h\left(\frac{\Omega_j}{T}\right)\right]+\delta^2\frac{\lambda^2N_j}{2}\frac{\Omega_j^2}{(4\pi)^4}\left(1+\frac{n^2}{2}\right)\left[7+\frac{\pi^2}{6}-6\gamma_E+2\gamma_E^2-2(3-2\gamma_E)\right.\\&\left.\times\ln\left(\frac{\Omega_j^2}{4\pi\mu^2}\right)+2\ln^2\left(\frac{\Omega_j^2}{4\pi\mu^2}\right)\right]-\delta^2\frac{\lambda^2N_j}{2}\frac{\Omega_j^2}{(4\pi)^4}\left[1+\frac{11}{8}n^2-\left(1+\frac{n^2}{2}\right)\ln(n^2)-\frac{1}{2}n^2\ln^2(n^2)\right.\\&\left.+\frac{(1-n^2)^2}{n^2}\left(\mathrm{Li}_2(1-n^2)-\frac{\pi^2}{6}\right)\right]-\delta^2\frac{\lambda^2N_j}{2}\frac{\Omega_i^2}{(4\pi)^4}\left\{\left[3-2\gamma_E-2\ln\left(\frac{\Omega_j^2}{4\pi\mu^2}\right)\right]\left(\frac{1}{4}+\ln(n^2)\right)\right\}\\&+\delta^2N_j\frac{\lambda^2T^2}{(4\pi)^2}\left\{h\left(\frac{\Omega_i}{T}\right)\left[\ln\left(\frac{\Omega_j^2}{4\pi\mu^2}\right)-2+\gamma_E\right]+2h\left(\frac{\Omega_j}{T}\right)\left[\ln\left(\frac{\Omega_i^2}{4\pi\mu^2}\right)-2+\gamma_E\right]\right\}\\&+\delta^2N_j\frac{\lambda^2T^2}{8(4\pi)^2}\left[2\ln\left(\frac{\Omega_i+2\Omega_j}{3T}\right)+5.0669\right],\end{aligned} \tag{3.33}$$

where $n=\Omega_i/\Omega_j$.

From Eqs. (3.6), (3.18)–(3.25), (3.28), (3.29), (3.32), and (3.33) one easily sees that all the temperature-dependent divergences cancel exactly. The remaining divergences are handled in the usual way, being canceled by the counterterms appearing in $\mathcal{L}_{\rm ct}$, Eq. (2.2) (see Appendix B). The sum of the remaining finite terms of each contribution to the self-energy makes the total contribution to the thermal mass up to order δ^2, $M_i^2=\Omega_i^2-\delta\eta_i^2+\Sigma_{i,1}+\cdots+\Sigma_{i,13}$.

IV. NUMERICAL RESULTS

We are now in position to set $\delta=1$ and apply the PMS to the thermal masses. Before doing that few points concerning the optimization procedure should be clarified. First, we recall that our interpolation procedure has been carried out in a very general way by assigning a different interpolation parameter to each field. Although general, this procedure brings in two arbitrary parameters which have to be fixed with the PMS. Of course this complicates the numerical optimization procedure, which is needed at higher orders, since one has to look for extrema in the η_1,η_2 space. Sometimes these extrema show up as saddle points which are hard to detect numerically. In principle, bearing in mind that ϕ_1 and ϕ_2 are both the same type of fields, one could be tempted to use the freedom allowed by the interpolating process to set $\eta_1=\eta_2=\eta$. In order to assess the validity of such choice we have done the optimization in both ways finding that the case $\eta_1\neq\eta_2$ gives better results. The second point regards the actual quantity to be extremized. By looking at our equations one can easily see that, except for the case where $N_1=N_2$, $m_1^2=m_2^2$ and $\lambda_1=\lambda_2$, the PMS applied separately to M_1^2 and M_2^2, at the same temperature, can generate different values for the same $\overline{\eta_i}$. One way to avoid this would be to evaluate and optimize a more comprehensive quantity such as the effective potential. In fact this procedure has been advocated in other applications of the optimized δ expansion [28]. However, in the present work we have not attempted to evaluate the effective potential since, at $\mathcal{O}(\delta^2)$, this would imply in the evaluation of three-loop zero point functions which become rather cumbersome at finite temperatures.[2] Although this may be regarded as a controversial point within the method it will not be discussed any further in the present application. Here we follow the original prescription given in Ref. [30] where it is suggested that the PMS should be applied to each different physical quantity so that η_i can be adjusted to the relevant energy scale. The validity of such procedure will be judged by comparing our results with well known predictions in the $N_1=N_2=1$ limit. Finally, as discussed in Ref. [20], one can easily see that applying the PMS to M_i^2 at first order in δ produces coupling independent values for $\overline{\eta_i}$ which do not furnish truly nonperturbative results. Therefore we will only investigate the results generated at order δ^2.

[2]See Ref. [33] for a discussion concerning the δ-expansion evaluation of the effective potential.

TABLE I. Results for the critical temperature as obtained in the one-loop approximation, the renormalization group approach in Ref. [14] and in the δ expansion, respectively.

λ_1	λ_2	λ	$T_c^{1\text{-loop}}/m_1$	$T_c^{\rm RGA}/m_1$	$T_c^{\delta^2}/m_1$
0.06	1.8	-0.1	24.5	33.6	33.3
0.0167	0.6	-0.025	53.7	67.9	66.9

We work in units of the arbitrary scale μ introduced by dimensional regularization, by extremizing the dimensionless quantity M_i^2/μ^2. To search for inverse symmetry breaking at high temperatures one must ensure that the symmetries are restored at $T=0$. This is achieved by setting $m_i^2>0$ and by observing the boundness condition while setting $\lambda\to-\lambda$ in all our equations.

A. The $Z_2\times Z_2$ case

Let us start by studying the $N_1=N_2=1$ case where the theory reduces to the $Z_2\times Z_2$ model which has been extensively studied in the literature. In Ref. [14] (see also Ref. [15]) it is claimed that the critical temperature is not reliably estimated by the loop expansion which does not include temperature effects in the coupling constants. On the other hand, the nonperturbative renormalization group approach (RGA) used in Ref. [14] does include those effects and as a first check of the validity of our results we estimate the critical temperature for the $Z_2\times Z_2$ model comparing our results at $\mathcal{O}(\delta^2)$ with the ones furnished by the two methods mentioned above. This is done in the first two rows of Table I and also in Fig. 1. In all cases $m_1^2/\mu^2=m_2^2/\mu^2=1.0$. Just above the critical temperatures presented in the first two rows the thermal mass M_1^2 is negative whereas M_2^2 is positive. Our numerical optimization strategy is the following: for a temperature below the value predicted by the one-loop

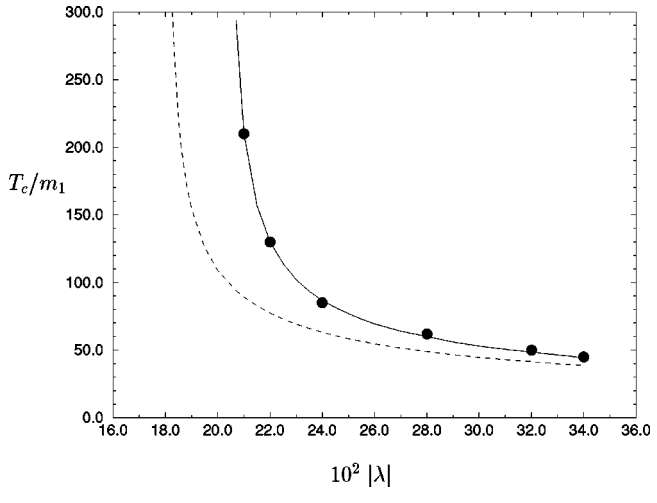

FIG. 1. The critical temperature T_c/m_1 as a function of λ (<0) for $N_1=1$ and $N_2=1$ with the following parameter values: $m_{1,2}^2/\mu^2=1.0$, $\lambda_1=0.018$, and $\lambda_2=0.6$. The dashed line is the one-loop prediction, the continuous line is our result and the dots represent the values obtained with the RGA.

approximation (1LA) we identify the extremum in the η_1, η_2 space. Both masses in the extremum positions are found to be consistently positive and the extremum positions are found to be unique (and consistent with the high-temperature approximation, in the sense that $\overline{\eta}_{1,2} < T$). The extremum is then followed as the temperature is increased. When one of the masses becomes negative the value of T_c is obtained and the values of $\overline{\eta}_1, \overline{\eta}_2$ are registered. For example, around the critical temperature the values obtained by extremizing M_1^2 are $\overline{\eta}_1 \approx 0$, $\overline{\eta}_2 \approx 0.25T$ and $\overline{\eta}_1 \approx 0$, $\overline{\eta}_2 \approx 0.15T$ for the parameters in the first and second rows, respectively, in Table I. From this table one can see the remarkable agreement between our results and the ones provided by the RGA. In Fig. 1 we compare the numerical values of the critical temperature with the ones predicted by the 1LA and RGA for several values of the cross coupling. Once again our results agree with the ones given by the RGA [14,15]. We have also investigated the behavior of the critical temperature as a function of λ_2 for fixed $m_{1,2}^2/\mu^2 = 1.0$, $\lambda_1 = 0.009$, and $\lambda = -0.025$. As can be seen directly from Eq. (2.4), the one-loop predicts that $T_c/m_1 \sim 49.0$ for any value of λ_2, while the RGA predicts that it increases with the latter. Once again our results, not shown, agree with the ones given by the RGA. These findings give us confidence about the correctness of the optimization procedure adopted.

The critical temperatures predicted by the δ expansion, as well as by the RGA, are higher than those predicted by the 1LA. This could be roughly understood by recalling that for the phase transitions considered the PMS applied to the mass which signals the phase transition (M_1^2 for the parameters of Table I) generates a $\overline{\eta}_2$ which is an increasing function of T whereas it gives $\overline{\eta}_1 \approx 0$. Therefore, at high T, the optimized mass $\overline{\Omega}_2$ which ''dresses'' the δ-expansion propagator associated with ϕ_2 is greater than its counterpart $\overline{\Omega}_1^2$. In M_1^2, the quantity $\overline{\Omega}_2^2$ is always associated with the coupling λ which drives ISB. It seems that the increasing of $\overline{\Omega}_2^2$ with the temperature suppresses the effect of λ in enhancing ISB. Another interesting point to be discussed regards the inclusion of temperature-dependent coupling constants. While this possible dependence is overlooked in the 1LA it is taken into account in the RGA. These effects are more subtle to be observed directly in our case. However, by looking at the nature of the diagrams considered by us at order δ^2, one may have an idea of how these effects enter our calculations. Basically, one can think of double scoops and setting suns diagrams as being tadpole diagrams with vertex corrections. Expanding the vertex to order δ gives the simple one loop diagrams considered in Eq. (3.11), while expanding the vertex to order δ^2 gives the double scoops and setting suns which indirectly contain one-loop temperature-dependent corrections to the vertex.

B. The $O(N_1) \times O(N_2)$ case

Let us now consider the more realistic $O(N_1) \times O(N_2)$ case. We follow Bimonte and Lozano, in the first citation in Ref. [11], by choosing $N_1 = 90$ and $N_2 = 24$ so that the model can be thought of as representing the Kibble-Higgs sector of a SU(5) grand unified model. Let us start by estimating some critical temperatures and comparing our results with the lowest order one-loop results given by Eqs. (2.4) and (2.5). The two first rows of Table II display our results for the set of parameters considered in the previous subsection. Our predicted values for the critical temperatures are proportionally much higher than for the $N_1 = N_2 = 1$ case. The two last rows of Table II display the results for more typical parameter values for this model, which are usually taken around $\lambda_1 = 0.8$ and $\lambda_2 = 1.0$ (see Ref. [4]). These results suggest that the parameter region for ISB predicted by the δ expansion is smaller than the one predicted by the lowest order 1LA prediction. To illustrate that we offer Figs. 2 and 3. Figure 2 shows our $\mathcal{O}(\delta^2)$ result (dot-dashed line) compared with the results produced by the 1LA at lowest order (thin continuous line) for fixed $\lambda_1 = 0.8$ and $T = 5.0\ \mu$. The upper parabola represents the limiting region for boundness. The dashed line is the Bimonte and Lozano's next to leading order one-loop (BLA) result for an arbitrarily large T. Figure 3 is similar to Fig. 2 except that λ_1 varies while λ_2 is kept fixed at the unity value. Note that the next to leading order correction considered in Ref. [11] for the one-loop approximation reduces significantly the region of ISB given at lowest order. However, the next to leading order calculation of the BLA ap-

TABLE II. Results for the critical temperature in the $O(90) \times O(24)$ scalar model.

λ_1	λ_2	λ	$T_c^{1\text{-loop}}/m_1$	$T_c^{\delta^2}/m_1$
0.06	1.8	-0.1	6.5	15.3
0.0167	0.6	-0.025	16.5	65.4
0.9	1.0	-0.141	2.2	5.0
0.8	0.7	-0.091	3.4	10.0

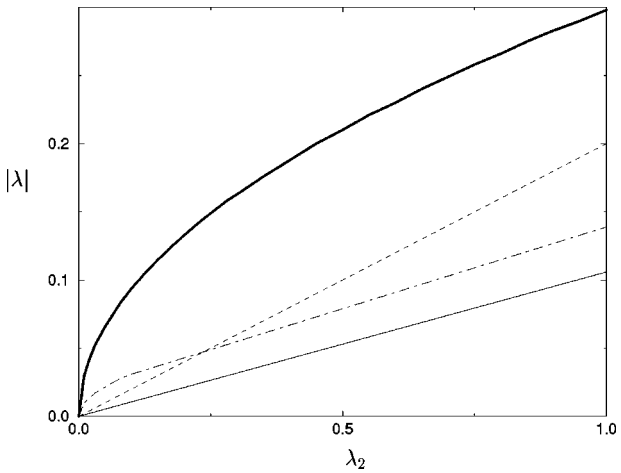

FIG. 2. Region of ISB at fixed $\lambda_1 = 0.8$ for $N_1 = 90$ and $N_2 = 24$. The thick parabola limits the region for which the potential is bounded. The continuous and dashed lines are the zeroth order (at $T/\mu = 5.0$) and first order (at an arbitrarily large T) results given in Ref. [11]. The dot-dashed line is our result at $T/\mu = 5.0$. The region of ISB is the one in between the boundness curve and the other curves for each case.

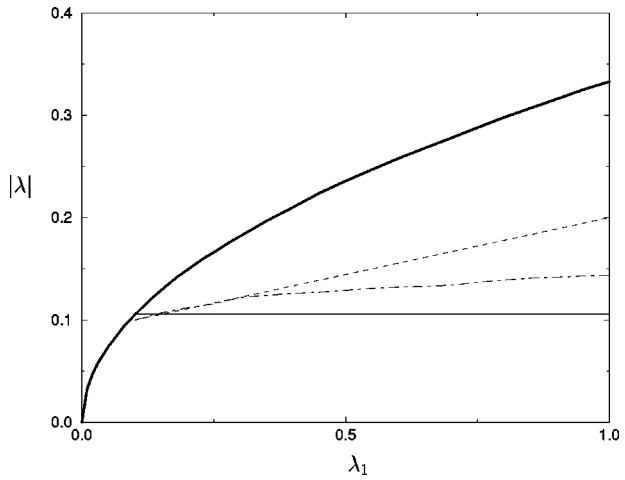

FIG. 3. Same as in Fig. 2, but now at fixed $\lambda_2=1.0$.

proach considers up to the second term, which is mass dependent, in the expansion of the temperature dependent integral given by Eq. (3.7). This means that their procedure does not take into account logarithmic terms in the expansion of $h(y_i)$ since they would give corrections of order $\lambda_i^2 \ln \lambda_i$ which also arise from two-loop diagrams. Our calculations, on the other hand, avoid these book-keeping problems and all contributions are consistently and explicitly considered in a given order. Moreover, support for ISB or SNR also arises in the work of Amelino-Camelia Ref. [12] who, similar to us, considers two-loop diagrams in the simple $Z_2 \times Z_2$ model.

To illustrate how the temperature affects the ISB region we offer Fig. 4 where we have fixed $\lambda_1=0.8$ while λ_2 varies. It is clear that the ISB parameter region for $T=5.0\ \mu$ is smaller than for $T=10.0\ \mu$. That is, increasing temperatures favor ISB. The parameter regions predicted by the 1LA have the same temperature dependence although the difference in size is less significant than the one displayed in Fig. 3 for the δ expansion.

Finally, let us investigate the possible patterns for ISB. According to the one-loop approach (to lowest and next to

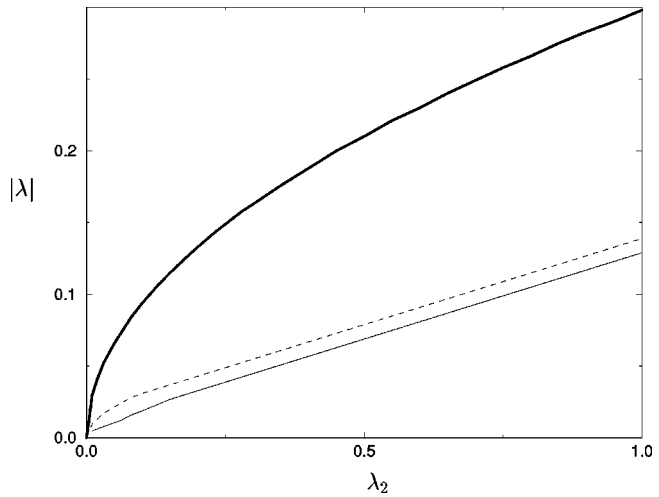

FIG. 4. The region of ISB for two different temperatures ($\lambda_1=0.8$) $T/\mu=5.0$ (dashed line) and $T/\mu=10.0$ (thin full line).

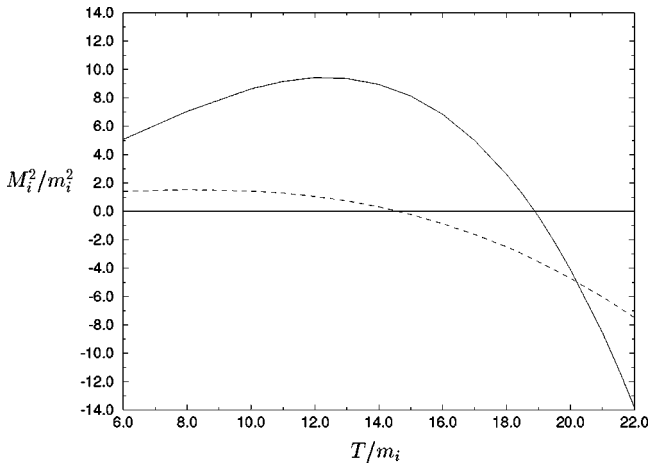

FIG. 5. The behavior of M_1^2 (dashed line) and M_2^2 (upper full line) as a function of the temperature for $\lambda_1=0.06$, $\lambda_2=1.8$, and $\lambda=-0.1$ ($N_1=90$ and $N_2=24$).

leading order) as well as to the RGA, there are only two possible phases at high T: either the theory is completely symmetric or one of the two symmetries is broken. However, including two-loop contributions and going beyond the simple perturbative expansion could alter this picture introducing a third possibility where the two symmetries are broken at high T. To analyze this possibility one must increase the temperature beyond the critical values shown in Tables I and II which display only the T_c connected with the phase transition from the symmetric phase to one of the nonsymmetric phases. Surprisingly we find, that for some parameter values, the mass associated with the symmetry which survives the first transition has a tendency to decrease as the temperature increases beyond the first critical value. As an example of this, we show in Fig. 5 the results for the case analyzed in the first row of Table II for both M_1^2 and M_2^2. M_2^2 is positive right above the critical temperature shown (now labeled T_{c1}) which is associated with the breaking in the ϕ_1 direction. We see that, very quickly, M_2^2 becomes monotonically decreasing with the temperature and becomes negative, through a second order phase transition, at $T_{c2}/m_2 \simeq 18.9$. The same behavior is observed for the parameters shown in the second row of Table II, where we observe symmetry breaking in ϕ_2 direction at $T_{c2}/m_2 \simeq 139$. However, analyzing the other two cases shown in the third and fourth rows of Table II, we find that the would be mass associated with the second symmetry breaking increases monotonically with the temperature, signalling that this symmetry possibly remains unbroken at high temperatures. A similar behavior happens for the two cases analyzed in Table I, for $N_1=N_2=1$. Although M_2^2 initially shows a decrease in value as the temperature is raised, it soon becomes monotonically increasing with T. Note that just by interchanging the values of λ_1 and λ_2 one trivially observes yet another pattern this time with $T_{c2}<T_{c1}$. Which pattern will be actually followed depends on our initial choice for the values of the couplings.

Therefore, our results suggest that a possible symmetry breaking along the second field direction takes place, for large values of N, in a narrow region of parameters. It is

possible that this alternative symmetry breaking pattern will show up only in nonperturbative calculations which consider up to two loop terms. It would be interesting to investigate this possibility using other nonperturbative approaches.

V. CONCLUSIONS

We have used the optimized linear δ expansion to investigate inverse symmetry breaking at high temperatures using multifield theories. Our order-δ^2 calculations take full consideration of two-loop contributions, including the momentum-dependent ''setting sun'' type of diagrams. To our knowledge, a complete calculation associated with the phenomenon of ISB or SNR which includes these contributions in the $O(N_1)\times O(N_2)$ model has not been fully considered before. In order to assure the reliability of the method we have started with the scalar $Z_2\times Z_2$ model which has been extensively investigated in connection with inverse symmetry breaking problem. We have shown that our optimized results agree well with those obtained with the renormalization group approach, especially as far as the critical temperatures are concerned. This has allowed us to establish the δ expansion as a reliable nonperturbative technique to investigate ISB. We have then investigated the more realistic scalar $O(N_1)\times O(N_2)$ model which may be related to the Kibble-Higgs sector of a SU(5) grand unified model. All our results strongly support the possibility of inverse symmetry breaking (or symmetry nonrestoration) at high temperatures. Surprisingly, we have also found evidence for a second phase transition taking place for some values of the couplings and large values of N. According to our results two other possible high temperature inverse symmetry breaking patterns are

$$O(N_1)\times O(N_2)\overset{T_{c1}}{\rightarrow}O(N_1-1)\times O(N_2)$$

$$\overset{T_{c2}}{\rightarrow}O(N_1-1)\times O(N_2-1),$$

where $T_{c1}<T_{c2}$ or

$$O(N_1)\times O(N_2)\overset{T_{c2}}{\rightarrow}O(N_1)\times O(N_2-1)$$

$$\overset{T_{c1}}{\rightarrow}O(N_1-1)\times O(N_2-1),$$

where $T_{c1}>T_{c2}$.

ACKNOWLEDGMENTS

R.O.R. was partially supported by CNPq.

APPENDIX A

Consider a general setting sun diagram given by ($d=4-2\epsilon$)

$$G_{ijj}(p)=\mu^{4\epsilon}\int\frac{d^dk}{(2\pi)^d}\int\frac{d^dq}{(2\pi)^d}\frac{1}{[k^2-\Omega_i^2+i\epsilon][q^2-\Omega_j^2+i\epsilon][(p-k-q)^2-\Omega_j^2+i\epsilon]}. \tag{A1}$$

At finite temperature we express the momentum integrals as in Eq. (3.3). The discrete sums in the Matsubara frequency can easily be done if we reexpress Eq. (A1) in terms of the Fourier transformed, in Euclidean time, expressions for the field propagators

$$G_{ijj}(\mathbf{p},i\omega_n)=\mu^{4\epsilon}\int\frac{d^{d-1}k_1}{(2\pi)^{d-1}}\frac{d^{d-1}k_2}{(2\pi)^{d-1}}\frac{d^{d-1}k_3}{(2\pi)^{d-1}}\times\int_0^\beta d\tau\, e^{i\omega_n\tau}G_i(\mathbf{k}_1,\tau)G_j(\mathbf{k}_2,\tau)G_j(\mathbf{k}_2,\tau)\times\delta^3(\mathbf{p}-\mathbf{k}_1-\mathbf{k}_2-\mathbf{k}_3), \tag{A2}$$

where $G_i(\mathbf{k},\tau)$ is the propagator, which can be written in terms of a spectral function $\rho(\mathbf{k},\eta)$, as

$$G_i(\mathbf{k},\tau)=\int_{-\infty}^{+\infty}\frac{d\eta}{2\pi}[1+n(\eta)]\rho_i(\mathbf{k},\eta)e^{-\eta|\tau|}, \tag{A3}$$

where n is the Bose distribution and

$$\rho_i(\mathbf{k},\eta)=\frac{2\pi}{2E_i(\mathbf{k})}\{\delta[\eta-E_i(\mathbf{k})]-\delta[\eta+E_i(\mathbf{k})]\}. \tag{A4}$$

Using Eq. (A3) in Eq. (A2), the identities $e^{i\beta\omega_n}=1$, $n(\eta)=e^{-\beta\eta}[1+n(\eta)]$, $n(\eta)=-[1+n(-\eta)]$ and performing the τ integration, we get

$$G_{ijj}(\mathbf{p},i\omega_n)=\mu^{4\epsilon}\int\frac{d^{d-1}k_1}{(2\pi)^{d-1}}\frac{d^{d-1}k_2}{(2\pi)^{d-1}}\frac{d^{d-1}k_3}{(2\pi)^{d-1}}\times\int_{-\infty}^{+\infty}\frac{d\eta_1}{2\pi}\frac{d\eta_2}{2\pi}\frac{d\eta_3}{2\pi}\times\rho_i(\mathbf{k}_1,\eta_1)\rho_j(\mathbf{k}_2,\eta_2)\rho_j(\mathbf{k}_3,\eta_3)\times[1+n(\eta_1)][1+n(\eta_2)][1+n(\eta_3)]\times\left[\frac{1}{i\nu_n+\eta_1+\eta_2+\eta_3}-\frac{1}{i\nu_n-\eta_1-\eta_2-\eta_3}\right]\times\delta^3(\mathbf{p}-\mathbf{k}_1-\mathbf{k}_2-\mathbf{k}_3). \tag{A5}$$

Performing the analytic continuation in the above expression $i\omega_n \to p_0 + i\epsilon$ and using

$$\lim_{\epsilon\to 0} \frac{\epsilon}{x^2+\epsilon^2} = \pi\delta(x), \tag{A6}$$

we can separate G_{ijj} in real and imaginary contributions, $G_{ijj} = \mathrm{Re}\, G_{ijj} + i\, \mathrm{Im}\, G_{ijj}$. The imaginary contribution gives the field decay rate and it is not important in the present work. The real part contributes to the thermal mass and it is given by [after performing the k_3 momentum integral with the help of the Dirac delta-function in Eq. (A5)]

$$\begin{aligned}
\mathrm{Re}\, G_{ijj}(\mathbf{p},p_0) = \int & \frac{d^{d-1}k_1}{(2\pi)^{d-1}} \frac{d^{d-1}k_2}{(2\pi)^{d-1}} \frac{\mu^{4\epsilon}}{8E_i(\mathbf{k}_1)E_j(\mathbf{k}_2)E_j(\mathbf{p}-\mathbf{k}_1-\mathbf{k}_2)} \\
& \times \int_{-\infty}^{+\infty} d\eta_1\, d\eta_3\, d\eta_3 \{\delta[\eta_1 - E_i(\mathbf{k}_1)] - \delta[\eta_1 + E_i(\mathbf{k}_1)]\}\{\delta[\eta_2 - E_j(\mathbf{k}_2)] \\
& - \delta[\eta_2 + E_j(\mathbf{k}_2)]\}\{\delta[\eta_3 - E_j(\mathbf{p}-\mathbf{k}_1-\mathbf{k}_2)] \\
& - \delta[\eta_3 + E_i(\mathbf{p}-\mathbf{k}_1-\mathbf{k}_2)]\}\left[\frac{1}{p_0+\eta_1+\eta_2+\eta_3} - \frac{1}{p_0-\eta_1-\eta_2-\eta_3}\right] \\
& \times \delta^3(\mathbf{p}-\mathbf{k}_1-\mathbf{k}_2-\mathbf{k}_3).
\end{aligned} \tag{A7}$$

After performing the η integrals with the help of the Dirac delta-functions and after some algebra, Eq. (A7) can be written in terms of three terms: a temperature-independent one, which is just the zero-temperature contribution $G_{ijj,0}$, and two other terms with one and two Bose factors, which gives the $G_{ijj,1}$ and $G_{ijj,2}$ terms appearing in Eq. (3.31).

The zero-temperature contributions in both cases have already been evaluated in the literature. The contribution $G_{iii,0}(p)$ has been evaluated in details in Refs. [34,35] where the quoted result for the on mass shell ($p^2 = \Omega_i^2$) case is

$$\begin{aligned}
G_{iii,0}(p) = & \frac{\Omega_i^2}{(4\pi^2)^4} \frac{\Gamma^2(1+\epsilon)}{(1-\epsilon)(1-2\epsilon)} \left(\frac{4\pi\mu^2}{\Omega_i^2}\right)^{2\epsilon} \\
& \times \left[-\frac{3}{2\epsilon^2} + \frac{1}{4\epsilon} + \frac{19}{8}\right],
\end{aligned} \tag{A8}$$

which gives

$$\begin{aligned}
G_{iii,0}(p) = & -\frac{3\Omega_i^2}{2(4\pi)^4}\left[\frac{1}{\epsilon^2} + \frac{3-2\gamma_E}{\epsilon} - \frac{2}{\epsilon}\ln\left(\frac{\Omega_i^2}{4\pi\mu^2}\right)\right] \\
& + \frac{p^2}{4(4\pi)^4\epsilon} - \frac{3\Omega_i^2}{(4\pi)^4}\left[\ln^2\left(\frac{\Omega_i^2}{4\pi\mu^2}\right)\right. \\
& \left. + \left(2\gamma_E - \frac{17}{6}\right)\ln\left(\frac{\Omega_i^2}{4\pi\mu^2}\right) + 1.9785\right],
\end{aligned} \tag{A9}$$

where we purposefully left the momentum dependence in the relevant divergent term to make explicit the need for a wave-function renormalization counterterm.

The zero-temperature contribution to the mixed setting sun diagram is also given in Ref. [35], for the on shell case ($p^2 = \Omega_i^2$) it can be written as

$$\begin{aligned}
G_{ijj,0}(p) = & \frac{\Omega_j^2}{(4\pi)^4} \frac{\Gamma^2(1+\epsilon)}{(1-\epsilon)(1-2\epsilon)} \left(\frac{4\pi\mu^2}{\Omega_j^2}\right)^{2\epsilon} \\
& \times \left\{-\frac{2+n^2}{2\epsilon^2} + \frac{n^2}{\epsilon}\left[\frac{1}{4} + \ln(n^2)\right]\right. \\
& + \left[1 + \frac{11}{8}n^2 - \left(1+\frac{n^2}{2}\right)\ln(n^2) - \frac{1}{2}n^2\ln^2(n^2)\right. \\
& \left.\left. + \frac{(1-n^2)^2}{n^2}\left(\mathrm{Li}_2(1-n^2) - \frac{\pi^2}{6}\right)\right]\right\},
\end{aligned} \tag{A10}$$

where $n = \Omega_i/\Omega_j$ and $\mathrm{Li}_2(z) = \Sigma_{l=1}^{\infty} z^l/l^2$. We then obtain the result

$$G_{ijj,0}(p)=-\frac{\Omega_j^2}{(4\pi)^4}\left\{\frac{1}{\epsilon^2}\left(1+\frac{n^2}{2}\right)+\frac{1}{\epsilon}\left(1+\frac{n^2}{2}\right)\left[3-2\gamma_E-2\ln\left(\frac{\Omega_j^2}{4\pi\mu^2}\right)\right]-\frac{p^2}{4\Omega_j^2\epsilon}-\frac{n^2}{\epsilon}\ln(n^2)\right\}$$
$$-\frac{\Omega_j^2}{(4\pi)^4}\left(1+\frac{n^2}{2}\right)\left[7+\frac{\pi^2}{6}-6\gamma_E+2\gamma_E^2-2(3-2\gamma_E)\ln\left(\frac{\Omega_j^2}{4\pi\mu^2}\right)+2\ln^2\left(\frac{\Omega_j^2}{4\pi\mu^2}\right)\right]$$
$$+\frac{\Omega_j^2}{(4\pi)^4}\left[1+\frac{11}{8}n^2-\left(1+\frac{n^2}{2}\right)\ln(n^2)-\frac{1}{2}n^2\ln^2(n^2)+\frac{(1-n^2)^2}{n^2}\left(\mathrm{Li}_2(1-n^2)-\frac{\pi^2}{6}\right)\right]$$
$$+\frac{\Omega_i^2}{(4\pi)^4}\left\{\left[3-2\gamma_E-2\ln\left(\frac{\Omega_j^2}{4\pi\mu^2}\right)\right]\left(\frac{1}{4}+\ln(n^2)\right)\right\}. \tag{A11}$$

The finite temperature terms $G_{ijj,1}$ and $G_{ijj,2}$ can be worked out as follows. Taking $\mathbf{p}=0$ in these terms, allows us to reexpress them by (using $\mathbf{k}_1\cdot\mathbf{k}_2=k_1k_2\cos\theta$)

$$\mathrm{Re}\,G_{ijj,1}(\mathbf{0},p_0)=\mu^{4\epsilon}\int\frac{d^{d-1}k_1}{(2\pi)^{d-1}}\frac{d^{d-1}k_2}{(2\pi)^{d-1}}\frac{1}{8E_i(\mathbf{k}_1)E_j(\mathbf{k}_2)}\frac{1}{k_1k_2}$$
$$\times\Bigg[n[E_i(\mathbf{k}_1)]\frac{\partial}{\partial\cos\theta}\ln(\{p_0^2-[E_i(\mathbf{k}_1)+E_j(\mathbf{k}_2)+E_j(\mathbf{k}_1+\mathbf{k}_2)]^2\}\{p_0^2-[-E_i(\mathbf{k}_1)+E_j(\mathbf{k}_2)+E_j(\mathbf{k}_1+\mathbf{k}_2)]^2\})$$
$$+2n[E_j(\mathbf{k}_2)]\frac{\partial}{\partial\cos\theta}\ln(\{p_0^2-[E_i(\mathbf{k}_1)+E_j(\mathbf{k}_2)+E_j(\mathbf{k}_1+\mathbf{k}_2)]^2\}$$
$$\times\{p_0^2-[E_i(\mathbf{k}_1)-E_j(\mathbf{k}_2)+E_j(\mathbf{k}_1+\mathbf{k}_2)]^2\})\Bigg] \tag{A12}$$

and

$$\mathrm{Re}\,G_{ijj,2}(\mathbf{0},p_0)=\mu^{4\epsilon}\int\frac{d^{d-1}k_1}{(2\pi)^{d-1}}\frac{d^{d-1}k_2}{(2\pi)^{d-1}}$$
$$\times\frac{1}{8E_i(\mathbf{k}_1)E_j(\mathbf{k}_2)}\frac{1}{k_1k_2}\times\{2n[E_i(\mathbf{k}_1)]n[E_j(\mathbf{k}_2)]+n[E_j(\mathbf{k}_1)]n[E_j(\mathbf{k}_1+\mathbf{k}_2)]\}$$
$$\times\frac{\partial}{\partial\cos\theta}\ln(\{p_0^2-[E_i(\mathbf{k}_1)+E_j(\mathbf{k}_2)+E_j(\mathbf{k}_1+\mathbf{k}_2)]^2\}\times\{p_0^2-[-E_i(\mathbf{k}_1)+E_j(\mathbf{k}_2)+E_j(\mathbf{k}_1+\mathbf{k}_2)]^2\}$$
$$\times\{p_0^2-[E_i(\mathbf{k}_1)-E_j(\mathbf{k}_2)+E_j(\mathbf{k}_1+\mathbf{k}_2)]^2\}\{p_0^2-[E_i(\mathbf{k}_1)+E_j(\mathbf{k}_2)-E_j(\mathbf{k}_1+\mathbf{k}_2)]^2\}). \tag{A13}$$

For $i=j$ (equal mass propagators) Eqs. (A12) and (A13) give the same expressions obtained by Parwani in Ref. [36]. In special, we note that, in Eq. (A12), the terms given by $\partial/\partial\cos\theta\ln\{\cdots\}\to 2k_1/k_2$ as $k_2\to\infty$. We can subtract and add this term in the appropriate places in Eq. (A12), obtaining the analogous expressions given by Parwani

$$-\frac{\lambda^2\delta^2N_j}{2}\mathrm{Re}\,G_{ijj,1}(\mathbf{0},p_0)=F_{ijj,0}+F_{ijj,1}+F_{ijj,2}(p_0), \tag{A14}$$

where

$$F_{ijj,0}=-\delta^2N_j\frac{\lambda^2T^2}{(4\pi)^2}\frac{1}{\epsilon}\left[h\left(\frac{\Omega_i}{T}\right)+2h\left(\frac{\Omega_j}{T}\right)\right] \tag{A15}$$

and

$$F_{ijj,1}=-\delta^2N_j\frac{\lambda^2T^2}{(4\pi)^2}\left\{h\left(\frac{\Omega_i}{T}\right)\left[-\ln\left(\frac{\Omega_j^2}{4\pi\mu^2}\right)+2-\gamma_E\right]\right.$$
$$\left.+2h\left(\frac{\Omega_j}{T}\right)\left[-\ln\left(\frac{\Omega_i^2}{4\pi\mu^2}\right)+2-\gamma_E\right]\right\}, \tag{A16}$$

where in the above equations, $h(y_i)$ is given by Eq. (3.10). The remaining terms, $F_{ijj,2}$ and $G_{ijj,2}$ can be evaluated on-shell and a similar contribution has already been computed earlier in the literature, see Ref. [37], from where we obtain

$$F_{ijj,2}(\Omega_i)-\frac{\lambda^2\delta^2 N_j}{2}\mathrm{Re}\,G_{ijj,1}(\mathbf{0},\Omega_i)$$

$$\sim-\delta^2 N_j^2\frac{\lambda^2 T^2}{8(4\pi)^2}\left[2\ln\left(\frac{\Omega_i+2\Omega_j}{3T}\right)+5.0669\right]. \tag{A17}$$

The finite temperature contributions $G_{iii,1}$ and $G_{iii,2}$ are given, as in Ref. [36] and, from the previous equations, Eqs. (A14)–(A17), they can be written as

$$-\delta^2\frac{\lambda_i^2(N_i+2)}{18}\mathrm{Re}[G_{iii,1}(\mathbf{0},\Omega_i)]=F_{iii,0}+F_{iii,1}+F_{iii,2}, \tag{A18}$$

where[3]

$$F_{iii,0}=-\delta^2\frac{\lambda_i^2(N_i+2)T^2}{3(4\pi)^2}\frac{1}{\epsilon}h\left(\frac{\Omega_i}{T}\right), \tag{A19}$$

$$F_{iii,1}=-\delta^2\frac{\lambda_i^2(N_i+2)T^2}{3(4\pi)^2}h\left(\frac{\Omega_i}{T}\right)\times\left[-\ln\left(\frac{\Omega_i^2}{4\pi\mu^2}\right)+2-\gamma_E\right], \tag{A20}$$

and

$$F_{iii,2}(\Omega_i)-\frac{\delta^2\lambda_i^2(N_i+2)}{18}\mathrm{Re}[G_2(\mathbf{0},\Omega_i)]$$

$$\sim\delta^2\frac{\lambda_i^2(N_i+2)T^2}{72(4\pi)^2}\left[\ln\left(\frac{\Omega_i^2}{T^2}\right)+5.0669\right]. \tag{A21}$$

Putting all these contributions together, we obtain the results given in Eqs. (3.32) and (3.33).

[3]Note that there is a misprint in Eq. (2.32) of Ref. [20], where there is an extra 1/2 multiplying that equation.

APPENDIX B

To obtain the total finite order δ^2 contribution one can add all divergences appearing in Eqs. (3.18)–(3.25), (3.28), (3.29), (3.32), and (3.33). As it can be easily seem all the temperature-dependent divergences cancel exactly and one is left with temperature-independent poles.

By looking at all terms which contribute to this order one can identify two classes. The first is composed by diagrams such as the ones described by Eqs. (3.20)–(3.25), (3.28), (3.29), (3.32), and (3.33). All of them are analogous to the diagrams which appear at second order in the couplings in the original theory and can be rendered finite by similar mass and wave-function counterterms. This procedure has already been illustrated at order δ. One can generalize this procedure by stating that diagrams belonging to a general order δ^n, and containing any combination $\lambda^m\lambda_1^k\lambda_2^l$ such that $m+k+l=n$ will be renormalized exactly as when ordinary perturbation theory is applied to the original model. Then, one just has to replace the original masses with the relevant interpolating masses $\Omega_{1,2}$. It is easy to check that for those diagrams the most divergent terms will display ϵ^{-n} poles.

The second kind of diagram is exclusive of the interpolated theory and carries at least one $\delta\eta_i^2$ (or $\delta\eta_j^2$) vertex. At $\mathcal{O}(\delta^2)$ these diagrams are described by Eqs. (3.18) and (3.19), which display the divergent η_i^2 and η_j^2 pieces. Looking at $\mathcal{L}_{\mathrm{ct}}^{\delta}$ one identifies a η_i^2,η_j^2-dependent coefficient whose Feynman rule is $i\delta B_i^{\delta}(\eta_1,\eta_2)$. Since the actual pole is of order-δ^2 one identifies this coefficient as having the same structure as the mass counterterm $B^{\delta^1}(\Omega_1,\Omega_2)$, displayed in Eq. (3.6), except that we now have $\eta_{i,j}^2$ instead of $\Omega_{i,j}^2$. Therefore, $\mathcal{O}(\delta^n)$ diagrams belonging to the second class will make use of the counterterm $\delta B^{\delta^n}(\eta_1,\eta_2)$. This coefficient is similar to $B^{\delta^{1-n}}(\Omega_1,\Omega_2)$ which has been evaluated in a previous order. One can also easily check that for these diagrams the most divergent terms will have ϵ^{n-1} poles. Moreover, power counting reveals that those $\delta\eta_i^2$ (or $\delta\eta_j$) insertions make the loops more convergent. For example, *all* one loop diagrams of order $\mathcal{O}(\delta^n)$, with $n\geqslant 3$ are finite.

The renormalization prescription adopted here is analogous to the one shown in Ref. [20] for the one-field case, where we have shown that the order by order renormalization holds at any higher orders in δ. In Ref. [20] the renormalization procedure is treated in more detail for the simple $\lambda\phi^4$ case.

[1] S. Weinberg, Phys. Rev. D **9**, 3357 (1974).

[2] R. N. Mohapatra and G. Senjanovic, Phys. Rev. Lett. **42**, 1651 (1979).

[3] S. Dodelson and L. M. Widrow, Phys. Rev. Lett. **64**, 340 (1990); S. Dodelson, B. R. Greene, and L. M. Widrow, Nucl. Phys. **B372**, 467 (1992).

[4] P. Salomonson, B.-S. Skagerstam, and A. Stern, Phys. Lett. **151B**, 243 (1985); P. Langacker and S.-Y. Pi, Phys. Rev. Lett. **45**, 1 (1980); G. Dvali and G. Senjanović, *ibid.* **74**, 5178 (1995); G. Dvali, A. Melfo, and G. Senjanović, *ibid.* **75**, 4559 (1996).

[5] J. Lee and I. Koh, Phys. Rev. D **54**, 7153 (1996).

[6] A. Riotto and G. Senjanović, Phys. Rev. Lett. **79**, 349 (1997); B. Bajc, A. Melfo, and G. Senjanović, Phys. Lett. B **387**, 796 (1996).

[7] Y. Fujimoto and S. Sakakibara, Phys. Lett. **151B**, 260 (1985); E. Manesis and S. Sakakibara, *ibid.* **157B**, 287 (1985); K. G. Klimenko, Theor. Math. Phys. **80**, 929 (1989); M. P. Grabowski, Z. Phys. C **48**, 505 (1990).

[8] G. A. Hajj and P. M. Stevenson, Phys. Rev. D **37**, 413 (1988);

K. G. Klimenko, Z. Phys. C **43**, 581 (1989).
[9] M. B. Gavela, O. Pène, N. Rius, and S. Vargas-Castrillón, Phys. Rev. D **59**, 025008 (1999).
[10] G. Bimonte, D. Iñiguez, A. Tarancón, and C. L. Ullod, Nucl. Phys. **B515**, 345 (1998); Phys. Rev. Lett. **81**, 750 (1998).
[11] G. Bimonte and G. Lozano, Phys. Lett. B **366**, 248 (1996); Nucl. Phys. **B460**, 155 (1996).
[12] G. Amelino-Camelia, Phys. Lett. B **388**, 776 (1996); Nucl. Phys. **B476**, 255 (1996).
[13] J. Orloff, Phys. Lett. B **403**, 309 (1997).
[14] T. Roos, Phys. Rev. D **54**, 2944 (1996).
[15] M. Pietroni, N. Rius, and N. Tetradis, Phys. Lett. B **367**, 119 (1997).
[16] K. Jansen and M. Laine, Phys. Lett. B **435**, 166 (1998); G. Bimonte, D. Iñiguez, A. Tarancón, and C. L. Ullod, Nucl. Phys. **B559**, 103 (1999).
[17] A. Okopińska, Phys. Rev. D **35**, 1835 (1987).
[18] A. Duncan and M. Moshe, Phys. Lett. B **215**, 352 (1988).
[19] V. I. Yukalov, Moscow Univ. Phys. Bull. **31**, 10 (1976); R. Seznec and J. Zinn-Justin, J. Math. Phys. **20**, 1398 (1979); J. C. LeGuillou and J. Zinn-Justin, Ann. Phys. (N.Y.) **147**, 57 (1983).
[20] M. B. Pinto and R. O. Ramos, Phys. Rev. D **60**, 105005 (1999).
[21] S. Chiku and T. Hatsuda, Phys. Rev. D **58**, 076001 (1998).
[22] A. Okopińska, Phys. Rev. D **36**, 2415 (1987).
[23] S. K. Gandhi and M. B. Pinto, Phys. Rev. D **49**, 4258 (1994).
[24] M. B. Pinto, Phys. Rev. D **50**, 7673 (1994).
[25] I. R. C. Buckley, A. Duncan, and H. F. Jones, Phys. Rev. D **47**, 2554 (1993); A. Duncan and H. F. Jones, *ibid.* **47**, 2560 (1993); C. M. Bender, A. Duncan, and H. F. Jones, *ibid.* **49**, 4219 (1994); C. Arvanitis, H. F. Jones, and C. S. Parker, *ibid.* **52**, 3704 (1995).
[26] R. Guida, K. Konishi, and H. Suzuki, Ann. Phys. (N.Y.) **249**, 109 (1996).
[27] S. K. Gandhi and A. J. McKane, Nucl. Phys. **B419**, 424 (1994).
[28] G. Krein, D. P. Menezes, and M. B. Pinto, Phys. Lett. B **370**, 5 (1996); G. Krein, R. S. M. Carvalho, D. P. Menezes, M. Nielsen, and M. B. Pinto, Eur. Phys. J. A **1**, 45 (1998).
[29] T. S. Evans, H. F. Jones, and A. Ritz, Nucl. Phys. **B517**, 599 (1998).
[30] P. M. Stevenson, Phys. Rev. D **23**, 2916 (1981).
[31] P. Ramond, *Field Theory: A Modern Primer* (Addison-Wesley, New York, 1990).
[32] J. Kapusta, *Finite Temperature Field Theory* (Cambridge University Press, Cambridge, England, 1985).
[33] S. K. Gandhi, H. F. Jones, and M. B. Pinto, Nucl. Phys. **B359**, 429 (1991).
[34] E. Mendels, Nuovo Cimento A **45**, 87 (1978).
[35] F. A. Berends, A. I. Davydychev, and N. I. Ussyukina, Phys. Lett. B **426**, 95 (1998); A. I. Davydychev and V. A. Smirnov, Nucl. Phys. **B554**, 391 (1999).
[36] R. R. Parwani, Phys. Rev. D **45**, 4695 (1992); **48**, 5965(E) (1993).
[37] P. Arnold and O. Espinosa, Phys. Rev. D **47**, 3546 (1993).